

NeuRoRA: Neural Robust Rotation Averaging

Pulak Purkait, Tat-Jun Chin, and Ian Reid

Australian Centre for Robotic Vision, Australian Institute for Machine Learning
The University of Adelaide, Australia

<https://github.com/pulak09/NeuRoRA>

Abstract

Multiple rotation averaging is an essential task for structure from motion, mapping, and robot navigation. The task is to estimate the absolute orientations of several cameras given some of their noisy relative orientation measurements. The conventional methods for this task seek parameters of the absolute orientations that agree best with the observed noisy measurements according to a robust cost function. These robust cost functions are highly nonlinear and are designed based on certain assumptions about the noise and outlier distributions. In this work, we aim to build a neural network that learns the noise patterns from the data and predict/regress the model parameters from the noisy relative orientations. The proposed network is a combination of two networks: (1) a view-graph cleaning network, which detects outlier edges in the view-graph and rectifies noisy measurements; and (2) a fine-tuning network, which fine-tunes an initialization of absolute orientations bootstrapped from the cleaned graph, in a single step. The proposed combined network is very fast, moreover, being trained on a large number of synthetic graphs, it is more accurate than the conventional iterative optimization methods. Although the idea of replacing robust optimization methods by a graph-based network is demonstrated only for multiple rotation averaging, it could easily be extended to other graph-based geometric problems, for example, pose-graph optimization.

1. Introduction

Recently, we have witnessed a surge of interest in applying neural networks in various computer vision and robotics problems, such as, single-view depth estimation [12], absolute pose regression [19] and 3D point-cloud classification [25]. However, we still rely on robust optimizations at different steps of geometric problems, for example, robot navigation and mapping. The reason is that neural networks have not yet proven to be effective in solving constrained optimization problems. Some classic examples of

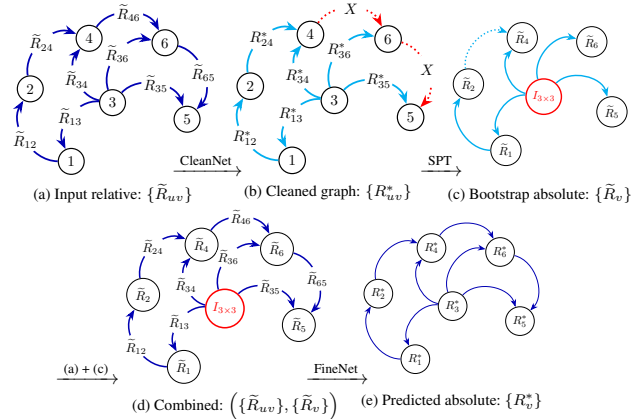


Figure 1. The proposed method NeuRoRA is a two-step approach: in the first step a graph-based network (CleanNet) is utilized to clean the view-graph by removing outliers and rectifying noisy measurements. An initialization from the cleaned view-graph, instantiated from a shortest path tree (SPT), is then further fine-tuned using a separate graph-based network (FineNet). The notations are outlined in Table 1.

the test-time geometric optimization include rotation averaging [5, 10, 11, 17, 28], pose-graph optimization [21], local bundle adjustment [24] and global structure from motion [29]. These optimization methods estimate the model parameters that agree best with the observed noisy measurements by minimizing a robust (typically non-convex) cost function. Often, these loss functions are designed based on certain assumptions about the sensor noise and outlier distributions. However, the observed noise distribution in a real-world application could be far from those assumptions. A few such examples of noise patterns in real datasets are displayed in Figure 2. Furthermore the nature and the structure of the objective loss function is the same for different problem instances of a specific task. Nonetheless, existing methods optimize the loss function for each instance. Moreover, an optimization during test-time could be slow for a target task involving a large number of parameters, and often forestalls a real-time solution to the problem.

In this work, with the advancement of machine learning,

we address the following question: “*can we learn the noise patterns in data, given thousands of different problem instances of a specific task, and regress the target parameters instead of optimizing them during test-time?*” The answer is affirmative for some specific applications, and we propose a learning framework that exceeds baseline optimization methods for a geometric problem. We choose *multiple rotation averaging* (MRA) as a target application to validate our claim. However, we believe that the idea could easily be extended to other robust optimization problems in geometric computer vision, and could lead to a new direction in research for an alternative of robust optimization methods.

In MRA, the task is to estimate the absolute orientations of cameras given some of their pairwise noisy relative orientations defined on a view-graph. There are a different number of cameras for each problem instance of MRA, and usually sparsely connected to each other. Further, the observed relative orientations are often corrupted by outliers. The conventional methods for this task [5, 10, 17, 28] optimize the parameters of the absolute orientations of the cameras that are most compatible (up to a robust cost function) with the observed noisy relative orientations.

We propose a neural network for robust MRA. Our network is a combination of two simple four-layered message-passing neural networks defined on the view-graphs. The first network cleans a view-graph by detecting outlier edges and rectifying noisy observations. An initialization of the absolute orientations is then commenced from a spanning tree of the cleaned view-graph. The second network then fine-tunes the initialization in a single step. Although a recurrent neural network that iteratively fine-tunes an initialization could also be an interesting choice, the proposed single-step refinement is already producing superior results for this task than the baselines optimization methods. The method is also summarized in Figure 1. We name our method *Neural Robust Rotation Averaging*, which is abbreviated as NeuRoRA in the rest of the manuscript.

Contribution and findings

- A graph-based neural network NeuRoRA is proposed as an alternative to conventional optimizations for MRA.
- NeuRoRA requires *no* explicit optimization at test-time and hence it is **much faster** (10 – 50× on CPUs and 500 – 2000× on GPUs) than the baseline optimizations.
- The proposed NeuRoRA is **more accurate** than the conventional optimization methods of MRA. The mean/median orientation error of the predicted absolute orientations by the proposed method is 1.45°/0.74°, compared to 2.17°/1.25° by an optimization method [5].
- Being a **small size** network, the proposed network is fast and can easily be deployed to real-world applications. The combined network (NeuRoRA) size is < 0.5Mb.

Further, the proposed method can potentially be tailored to other geometric problems, for example, **pose-graph** opti-

mization, with the inclusion of absolute locations of the cameras with additional sensor measurements, *e.g.* GPS.

2. Related works

We separate the related methods into two separate sections—(i) learning based methods as an alternative to optimizations, and (ii) relevant optimizations specific to MRA. (i) **Learning to optimize** A neural network is proposed as an alternative to non-linear least square optimizations in [8] for camera tracking and mapping. It exploits the least square structure of the problem and uses a recurrent network to compute updated steps of the optimization variables. In a similar direction, [23] relaxes the assumptions made by inverse compositional algorithms for dense image alignment by incorporating data-driven priors. [26] proposes a bundle adjustment layer that learns to predict the dampening parameter of the Levenberg-Marquardt algorithm to optimize depth and camera parameters. In contrast to the direct optimization-based methods that explicitly use regularizers to solve an ill-posed problem, [1] implicitly learn the prior through a data-driven method. Aoki *et al.* [3] proposed an iterative algorithm based on PointNet [25] for point-cloud registration as an alternative to direct optimization. Learning to predict an approximate solution to combinatorial optimization problem over graphs, *e.g.* minimum vertex cover, traveling salesman problem, *etc.*, is proposed in [20]. Learning methods to optimize general black-box functions [7] have also received a lot of attention recently. These conventional learning-based methods are tailored to some specific problems, where in this work, we are interested in an alternative learning-based solution for geometric problems, *e.g.* SFM.

(ii) **Robust optimization for rotation averaging** MRA was first introduced in [14] where a linear solution was proposed using quaternion averaging and later in [15] using Lie group based averaging. The solutions were non-robust in both the cases. Recently, there has been progress in designing robust algorithms [6, 16] for rotation averaging. Most of the algorithms are based on iterative methods for optimizing a robust loss function. They initialize the solution from a spanning tree and iteratively fine-tune it by minimizing a robust ℓ_1 or $\ell_{\frac{1}{2}}$ loss function. The state of the art approaches for robust MRA are listed below:

- Chatterjee and Govindu [5] fine-tune an initialization by first performing an iterative ℓ_1 minimization, followed by another iterative reweighted least squares with a more robust loss function $\ell_{\frac{1}{2}}$.
- Hartley *et al.* [16] propose a straight-forward method. It fine-tunes an initialization by the Weiszfeld algorithm of ℓ_1 averaging [4]. At every iteration, the absolute orientations of each camera are updated by the median of those computed from its neighbors.
- DISCO [9] employs a two-step approach. In the first

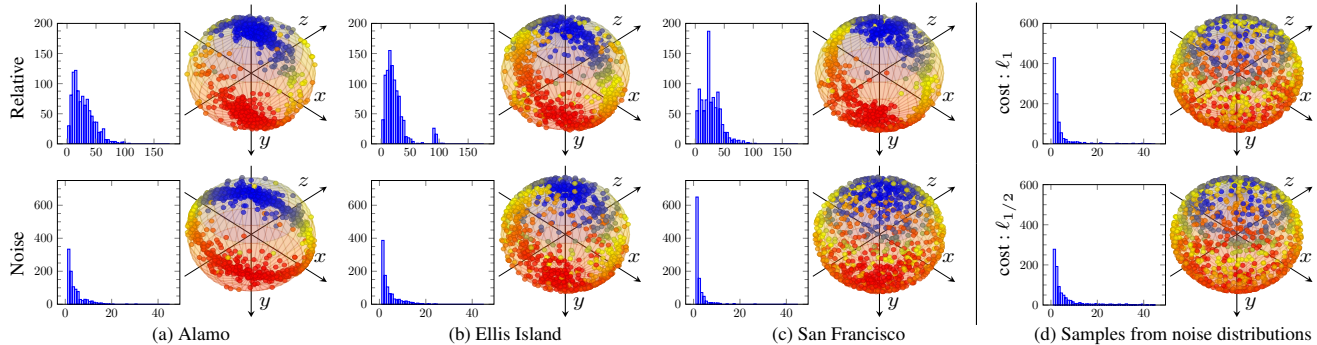


Figure 2. The angle and axes of sampled observed relative orientations (first row) and the same of noise (second row) in real datasets (for clarity only 1000 random samples) are displayed. The view-graphs of (a)-(b) are shared by [29] and (c) is shared by [9]. The noise orientation is calculated from the ground-truth absolute orientations and the observed relative orientations. We plotted histograms of the magnitudes of the angles in degrees and the axes of the orientations. Notice that the axes of the sampled relative and noise orientations are distributed mostly along a vertical ring rather than uniformly on a unit ball. These relative orientation patterns (vertical axes) are not utilized by the optimization methods and further the sampled noise orientations (somewhat vertical axes) are far from the typical distribution assumptions regarded by optimization algorithms subject to the cost functions. Samples from such noise distributions are shown in (d).

step, the parameter space of the orientations is divided into a discrete set of smaller bins and pairwise camera constraints are formulated by a Markov random field. A loopy belief propagation is then used for an initial estimation of the absolute orientations. In the second step, a Levenberg-Marquardt method is employed with additional constraints to fine-tune the initial orientations.

3. Multiple rotation averaging

Consider N cameras with M pairwise relative orientation measurements forming a directed view-graph $\mathcal{G} = (\mathcal{V}, \mathcal{E})$. A vertex $\mathcal{V}_v \in \mathcal{V}$ corresponds to the absolute orientation \hat{R}_v (to be estimated) of the v th camera and an edge $\mathcal{E}_{uv} \in \mathcal{E}$ corresponds to the observed relative orientation \tilde{R}_{uv} from u th camera to v th camera. Conventionally, the task is to estimate the absolute orientations $\{\hat{R}_v\}$, with respect to a global reference of orientations, such that the estimated orientations are most consistent with the observed noisy relative orientation measurements, *i.e.* $\tilde{R}_{uv} \approx \hat{R}_v \hat{R}_u^{-1}, \forall \mathcal{E}_{uv} \in \mathcal{E}$. Further, the observed measurements are corrupted by outliers, *i.e.* some of the orientations \tilde{R}_{uv} are far from $\hat{R}_v \hat{R}_u^{-1}$. Conventionally, the solution is obtained by minimizing a robust cost function that penalizes the discrepancy between observed noisy relative orientations $\{\tilde{R}_{uv}\}$ and the estimated relative orientations $\{R_{uv}^*\} := \{\hat{R}_v \hat{R}_u^{-1}\}$. The corresponding optimization problem can then be expressed as

$$\arg \min_{\{R_v^*\}} \sum_{\mathcal{E}_{uv} \in \mathcal{E}} \rho(d(R_{uv}^*, \tilde{R}_{uv})) \quad (1)$$

where $\rho(\cdot)$ is a robust cost and $d(\cdot, \cdot)$ is a distance measure between the orientations. The distance measures include geodesic, quaternion and chordal [17] metrics (described

below). The cost function $\rho(\cdot)$ is designed according to the assumption of sensor noise and outlier distribution by the optimization method (described below in detail). The nature of the above optimization is a typical complex multi-variable nonlinear optimization problem with thousands of variables (for thousands of cameras) and there seems to be no direct method (closed-form solution) minimizing the above cost even without outliers [17].

The choice of distance measure $d(\tilde{R}, R)$ There are three commonly used distance measurements in the rotation group $\text{SO}(3)$: (1) the geodesic or angle metric $d_\theta = \angle(\tilde{R}, R)$, (2) the chordal metric $d_C = \|\tilde{R} - R\|_F$ and (3) the quaternion metric $d_Q = \min\{\|q_{\tilde{R}} - q_R\|, \|q_{\tilde{R}} + q_R\|\}$ where q_R and $q_{\tilde{R}}$ are quaternion representations of R and \tilde{R} respectively, and $\|\cdot\|_F$ is the Frobenius norm. Note that q_R and $-q_R$ represent the same orientation. The metrics d_C and d_Q are proven to be $2\sqrt{2} \sin(d_\theta/2)$ and $2 \sin(d_\theta/4)$ respectively [17], thus, all the metrics are the same to the first order. In our implementation, we employ the quaternion representations (with non-negative scalars) while designing the network and the loss functions.

The choice of robust cost $\rho(\cdot)$ In practical applications, *e.g.* robot navigation, the agent usually ends up with some corrupt measurements (outliers), due to symmetric and repetitive man-made structures, in addition to the sensor noise. To estimate the absolute orientations of the cameras that are immune to those outliers, the conventional methods optimize a robust cost $\rho(\cdot)$ as discussed above. An exhaustive list of such robust functions can be found in [5]. Specifically, Geman-McClure or $\ell_{\frac{1}{2}}$ are more robust to outliers than ℓ_1 or Huber loss, but prone to converge to a local minimum, and require a better initialization. Chatterjee *et al.* [5] refines the initialization utilizing a weighted ℓ_1 cost and further fine-tunes the solution employing an $\ell_{\frac{1}{2}}$ robust

Table 1. The notations used in the manuscript

Orientation parameters of the cameras in the view-graph	
\tilde{R}_{uv} : Observed relative	\tilde{R}_v : Initial absolute
R_{uv}^* : Noise rectified relative	R_v^Φ, R_v^* : Refined / predicted absolute
\hat{R}_{uv} : Ground-truth relative	\hat{R}_v : Ground-truth absolute
$\{R_{uv}\}$: Set of all relative	$\{R_v\}$: Set of all absolute
The network parameters / symbols	
α_{uv}^* : Predicted outlier score	$\hat{\alpha}_{uv}$: Ground-truth outlier score
$h_v^{(t)}$: Features at node v	$m_v^{(t)}$: Message at node v
\square : Permutation invariant op.	$\gamma^{(t)}$: Feature update at layer (t)
$\phi^{(t)}(h_v^{(t-1)}, h_u^{(t-1)}, e_{uv})$: Accumulated message for the edge \mathcal{E}_{uv}
lp_1, lp_2, lp_3	: Single layers of linear perceptrons

cost. Hartley *et al.* [16] employs a successive ℓ_1 averaging scheme to estimate the orientation of each camera in turn, given its neighbors. The noise and outliers in the observed relative orientations is assumed to follow some distributions subject to the cost function with mean identity orientation. However, in real data, we observe very different noise distributions and a few such examples are shown in Figure 2. Further, optical axis of most of the cameras are horizontal and hence the axes of the relative orientations are vertical. By training a neural network to perform the task, our aim is for the neural network to capture these patterns while predicting the absolute orientations.

4. Learning to predict absolute orientations

Let $\mathcal{D} := \{\mathcal{G}\}$ be a dataset of ground-truth view-graphs. Each view-graph $\mathcal{G} := (\mathcal{V}, \mathcal{E})$ contains a noisy relative orientation measurement \tilde{R}_{uv} for each edge $\mathcal{E}_{uv} \in \mathcal{E}$ and a ground-truth absolute orientation \hat{R}_v for each camera $\mathcal{V}_v \in \mathcal{V}$. The desired neural network learns a mapping Φ that takes noisy relative measurements $\{\tilde{R}_{uv}\}$ as input and predicts the absolute orientations $\{R_v^\Phi\} := \Phi(\{\tilde{R}_{uv}\})$ as output. To train the parameters of such network, one could minimize the discrepancy between the ground-truth $\hat{R}_{uv} := \hat{R}_v \hat{R}_u^{-1}$ and the estimated $R_{uv}^\Phi := R_v^\Phi R_u^{\Phi^{-1}}$ relative orientations (*cf.* equation (1)), *i.e.*

$$\arg \min_{\Phi} \sum_{\mathcal{G} \in \mathcal{D}} \sum_{\mathcal{E}_{uv} \in \mathcal{E}} d(R_{uv}^\Phi, \hat{R}_{uv}) \quad (2)$$

In contrast to (1), where conventional methods optimize the orientation parameters for each instance of the view-graph $\mathcal{G} \in \mathcal{D}$, here in (2), the network parameters are optimized during training that learn the mapping Φ effectively from observed relative orientations $\{\tilde{R}_{uv}\}$ to the target absolute orientations $\{\hat{R}_v\}$, *i.e.* $\{\hat{R}_v\} \approx \Phi(\{\tilde{R}_{uv}\})$ over the entire dataset of view-graphs \mathcal{D} .

Difficulty in direct training of Φ and gauge freedom For an arbitrary orientation R ,

$$R_{uv}^* := R_v^* R_u^{*-1} = (R_v^* R) (R_u^* R)^{-1}, \quad \forall \mathcal{E}_{uv} \in \mathcal{E} \quad (3)$$

Therefore, $\{R_v^*\}$ and $\{R_v^* R\}$ essentially represent the same solution to the MRA problem (1) and there is a gauge freedom of degree 3. The mapping Φ is thus one-to-many as $\{R_v^\Phi\}$ and $\{R_v^\Phi R\}$ correspond to the same cost (2). This gauge freedom makes it difficult to train such a network. Further, one could choose a direct cost (no associated gauge freedom) to learn an one-to-one mapping Φ , *e.g.*

$$\arg \min_{\Phi} \sum_{\mathcal{G} \in \mathcal{D}} \sum_{\mathcal{V}_v \in \mathcal{V}} d(R_v^\Phi, \hat{R}_v) \quad (4)$$

where the reference orientation is fixed according to the ground-truth. Again, $\{\hat{R}_v\}$ and $\{\hat{R}_v R\}$ represent the same ground-truth where the reference orientations are fixed at different directions. One could fix the issue by fixing the reference orientation to the orientation of the first camera in all the view-graphs in \mathcal{D} . However, in a graph (set representation), the nodes are permutation invariant. Thus the choice of the first camera, and hence the reference orientation, is arbitrary. Therefore, one needs to pass the reference orientation or the index of the first camera (possibly via a binary encoding) to the network as an additional input to be able to train such a network. However, we employ an alternative strategy adopted from the conventional optimization methods [5, 17], *i.e.* initialize a solution of the absolute orientations under a fixed reference and pass the initialization to the network to fine-tune the solution. The network gets the reference orientation as an additional input via initialization (see Figure 1(d)) and regress the parameters, *i.e.* $\{\hat{R}_v\} \approx \Phi(\{\tilde{R}_{uv}\}, \{\hat{R}_v\})$. Further, we train the network by minimizing a combined cost where the first term (2) enforces the consistency over the entire graph and the second term (4) enforces a unique solution, *i.e.*

$$\arg \min_{\Phi} \sum_{\mathcal{G} \in \mathcal{D}} \left(\sum_{\mathcal{E}_{uv} \in \mathcal{E}} d(R_{uv}^\Phi, \hat{R}_{uv}) + \beta \sum_{\mathcal{V}_v \in \mathcal{V}} d(R_v^\Phi, \hat{R}_v) \right) \quad (5)$$

where β is a weight parameter. Note that the reference orientation are now fixed at the orientation of a certain camera c in the initialization $\{\tilde{R}_v\}$ as well as in the ground-truth absolute orientations $\{\hat{R}_v\}$. Although, the choice of c is not critical, in practice, the camera c with most neighboring cameras is chosen as the reference, *i.e.* $\tilde{R}_c = \hat{R}_c = I_{3 \times 3}$.

The above mapping Φ is now one-to-one. However, it requires an initialization $\{\hat{R}_v\}$ as an additional input. Conventional methods initialize the absolute orientations using a spanning tree of the view graph. However even a single outlier in that spanning tree can lead to a very poor initialization, so it is very important to identify these outliers beforehand. Further, noise in the relative orientation along each edge of the spanning tree will also propagate at the subsequent nodes while computing the initial absolute orientations. Thus, we first clean the view-graph by removing

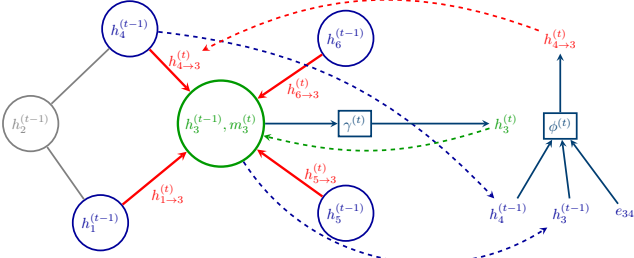


Figure 3. An illustration of computing next level features of a message-passing neural network.

the outliers and rectifying the noisy measurements, and then bootstrap an initialization from the cleaned view-graph.

Cleaning the view-graph Given the local structure in the view-graph, *i.e.* measurements of all the edges that the pair of adjacent nodes $\{\mathcal{V}_u, \mathcal{V}_v\}$ are connected to (and possibly subsequent edges), an outlier edge \mathcal{E}_{uv} can be detected. To be specific, chaining the relative orientations along a cycle in the local structure of the view-graph forms an orientation close to the identity orientation and an indication of an outlier in the cycle otherwise. The presence of an outliers in multiple such cycles through the current edge indicates that the edge to be an outlier. Furthermore, the amount of noise in a relative measurement \tilde{R}_{uv} can also be estimated. Instead of designing such explicit algorithms, we use another graph neural network to clean the graph. The proposed method can be summarized as follows:

- A graph-based network is employed to clean the view-graph by removing outlier measurements and rectifying noisy measurements (see Section 4.2).
- The cleaned view-graph can then be utilized to initialize the absolute orientations (see Section 4.3).
- The initialization is further fine-tuned using a separate graph-based network (see Section 4.4).

In summary and for clarity of the rest of the paper, the notations are outlined in Table 1.

4.1. The network design choice

Generalizing convolution operators to irregular domains, such as graphs, is typically expressed as neighborhood aggregation or a message-passing scheme. The proposed network is built using such Message-Passing Neural Networks (MPNN) [13], directly operating on view-graphs \mathcal{G} . A MPNN is defined in terms of message functions $m_v^{(t)}$ and update functions $\gamma^{(t)}$ that run for T time-steps (layers). At each time-step, the hidden state $h_v^{(t)}$ at each node (feature) in the graph is updated according to

$$h_v^{(t)} = \gamma^{(t)}(h_v^{(t-1)}, m_v^{(t)}) \quad (6)$$

where $m_v^{(t)}$ is the condensed message at node v , coming from the neighboring nodes $u \in \mathcal{N}_v$, and can be expressed

as follows:

$$m_v^{(t)} = \square_{\mathcal{V}_u \in \mathcal{N}_v} \phi^{(t)}(h_v^{(t-1)}, h_u^{(t-1)}, e_{uv}) \quad (7)$$

where \square denotes a differentiable, permutation invariant symmetric function, *e.g.* *mean*, *soft-max*, *etc.*, $\gamma^{(t)}$ and $\phi^{(t)}$ are concatenation operations followed by 1-D convolutions and ReLUs, e_{uv} is the edge feature of the edge \mathcal{E}_{uv} , $h_{u \rightarrow v}^{(t)} := \phi^{(t)}(h_v^{(t-1)}, h_u^{(t-1)}, e_{uv})$ is the accumulated message for the edge \mathcal{E}_{uv} at time-step (t) , and \mathcal{N}_v is the set of all neighboring cameras connected to \mathcal{V}_v . A diagram of the elements involved in computing the next-level features of a node is displayed in Figure 3.

4.2. View-graph cleaning network

The view-graph cleaning network (CleanNet) is built on a MPNN. The input to CleanNet is a noisy view-graph and the output is a clean one, *i.e.* the network takes noisy relative orientations \tilde{R}_{uv} as the edge features e_{uv} and predicts the noise-rectified relative orientations R_{uv}^* from the accumulated message $h_{u \rightarrow v}^{(T)} := \phi^{(T)}(h_v^{(T-1)}, h_u^{(T-1)}, e_{uv})$ at the last layer. It also predicts a score α_{uv}^* depicting the probability of the edge \mathcal{E}_{uv} to be an outlier. *i.e.*

$$R_{uv}^* = lp_1(h_{u \rightarrow v}^{(T)}) \star \tilde{R}_{uv} \quad \text{and} \quad \alpha_{uv}^* = lp_2(h_{u \rightarrow v}^{(T)}) \quad (8)$$

where $lp_1(\cdot)$ and $lp_2(\cdot)$ are single-layered linear perceptrons that map the accumulated messages to the edge noise orientation and outlier score respectively. \star is the matrix multiplication. The hidden states are initialized by null vectors, *i.e.* $h_v^{(0)} = \emptyset$. Note that instead of directly estimating the rectified orientations, we predict the noise in the relative orientation measurements, which are then multiplied to obtain the rectified orientations. The loss is chosen as the weighted combination of mean orientation error \mathcal{L}_{mre} of the rectified R_{uv}^* and ground-truth $\hat{R}_{uv} := \hat{R}_v \hat{R}_u^{-1}$ relative orientations, and mean binary cross-entropy error \mathcal{L}_{bce} of the predicted α_{uv}^* and the ground-truth outlier score $\hat{\alpha}_{uv}$, *i.e.*

$$\mathcal{L} = \sum_{\mathcal{G} \in \mathcal{D}} \sum_{\mathcal{E}_{uv} \in \mathcal{E}} \left(\mathcal{L}_{mre}(R_{uv}^*, \hat{R}_{uv}) + \lambda \mathcal{L}_{bce}(\alpha_{uv}^*, \hat{\alpha}_{uv}) \right) \quad (9)$$

where λ is a weight parameter (fixed as $\lambda = 10$). We formulate the orientations using unit quaternions and the predictions are normalized accordingly. The error in the prediction is also normalized by the degree of the node, *i.e.*

$$\mathcal{L}_{mre}(R_{uv}^*, \hat{R}_{uv}) = \frac{1}{|\mathcal{N}_v| |\mathcal{N}_u|} d_Q \left(\frac{R_{uv}^*}{\|R_{uv}^*\|_2}, \hat{R}_{uv} \right) \quad (10)$$

Experimentally, we observed the above loss produces superior performance than the standard discrepancy loss (2). Note that the ground-truth outlier score $\hat{\alpha}_{uv}$ is generated based on the amount of noise in the relative orientations.

Specifically, if the amount of noise in the relative orientation $\tilde{R}_v^{-1}\tilde{R}_{uv}\tilde{R}_u > 20^\circ$, the ground-truth edge label is assigned as an outlier, *i.e.* $\hat{\alpha}_{uv} = 1$ and $\hat{\alpha}_{uv} = 0$ otherwise.

An edge \mathcal{E}_{uv} is marked as an outlier edge if the predicted outlier score α_{uv}^* is greater than a predefined threshold ϵ . In all of our experiments, we choose the threshold $\epsilon = 0.75$ ¹. A cleaned view-graph \mathcal{G}^* is then generated by removing outlier edges from \mathcal{G} and replacing noisy relative orientations \tilde{R}_{uv} by the rectified orientations R_{uv}^* . Note that the cleaned graph \mathcal{G}^* is only employed to bootstrap an initialization of the absolute orientations.

4.3. Bootstrapping absolute orientations

Hartley *et al.* [16] proposed generating a spanning tree by setting the camera with the maximum number of neighbors as the root and recursively adding adjacent cameras without forming a cycle. The reference orientation is fixed at the camera at the root of the spanning tree. The orientations of the rest of the cameras in the tree are computed by propagating away the rectified orientations R_{uv}^* from the root node along the edges, *i.e.* $\tilde{R}_v = R_{uv}^*\tilde{R}_u$.

As discussed before, the noise in the relative orientation along each edge $R_{uv}^*\tilde{R}_{uv}^{-1}$ propagates at the subsequent nodes while computing the initial absolute orientations of the cameras. Therefore, the spanning tree that minimizes the sum of depths of all the nodes (also known as shortest path tree [27]) is the best spanning tree for the initialization. Starting with a root node, a shortest path tree could be computed by greedily connecting nodes to each neighboring node in the breadth-first order. The best shortest path tree can be found by applying the same procedure with each one of the nodes as a root node (time complexity $\mathcal{O}(n^2)$) [18]. However, we employed the procedure just once (time complexity $\mathcal{O}(n)$) with the root at the node with the maximum number of adjacent nodes (similar to Hartley *et al.* [16]) and observed similar results as with the best spanning tree. The reference orientation of the initialization and the ground-truth is fixed at the root of the tree. This procedure is very fast and it takes only a fraction of a second for a large view-graph with thousands of cameras. We abbreviate this procedure as SPT and it is the default initializer in all of our experiments.

4.4. Fine-tuning network

The fine-tuning network (FineNet) is again built on a MPNN. It takes the initial absolute orientations $\{\tilde{R}_v\}$ and the relative orientation measurements $\{\tilde{R}_{uv}\}$ as inputs, and predicts the refined absolute orientations $\{R_v^*\}$ as the output. The refined orientations are estimated from the hidden states $h_v^{(T)}$ of the nodes at the last layer of the network, *i.e.*

$$R_v^* = lp_3(h_v^{(T)}) \star \tilde{R}_v \quad (11)$$

¹The choice is not critical in the range $\epsilon \in [0.35, 0.8]$.

where lp_3 is a single layer of linear perceptron. We initialize the hidden states of the MPNN by the initial orientations, *i.e.* $h_v^{(0)} = \tilde{R}_v$. The edge attributes are chosen as the relative discrepancy of the initial and the observed relative orientations, *i.e.* $e_{uv} = \tilde{R}_v^{-1}\tilde{R}_{uv}\tilde{R}_u$. The loss for the fine-tuning network is computed as the weighted sum of edge consistency loss and the rotational distance between the predicted orientation \tilde{R}_v and the ground-truth orientation R_v , *i.e.*

$$\mathcal{L} = \sum_{\mathcal{G} \in \mathcal{D}} \left(\sum_{\mathcal{E}_{uv} \in \mathcal{E}} \mathcal{L}_{mre}(R_{uv}^*, \hat{R}_{uv}) + \frac{\beta}{|\mathcal{N}_v|} \sum_{v_v \in \mathcal{V}} d_Q \left(\frac{R_v^*}{\|R_v^*\|}, \hat{R}_v \right) \right) \quad (12)$$

where \mathcal{L}_{mre} is chosen as the quaternion distance (10). This is a combination of two loss functions chosen according to (5). We value consistency of the entire graph (enforced via relative orientations in the first term) over individual accuracy (second term), and so choose $\beta = 0.1$.

4.5. Training

The view-graph cleaning network and the fine-tuning network are trained separately. For each edge \mathcal{E}_{uv} in the view-graph with observed orientation \tilde{R}_{uv} , an additional edge \mathcal{E}_{vu} is included in the view-graph in the opposite direction with orientation $\tilde{R}_{vu} := \tilde{R}_{uv}^{-1}$. This will ensure the messages flow in both directions of an edge. In both of the above networks, the parameters are chosen as: the number of time-steps $T = 4$, the permutation invariant function \square as the *mean*, and the dimensions of the message $m_v^{(t)}$ and hidden state $h_v^{(t)}$ are 32.

The proposed networks are implemented in PyTorch ToolBox² and trained on a GTX 1080 Ti GPU with a learning rate of 0.5×10^{-4} and weight decay 10^{-4} . Each of CleanNet and FineNet are trained for 250 epochs (takes $\sim 4 - 6$ hours) to learn the network parameters. To prevent the networks from over-fitting on the training dataset, we randomly drop 25% of the edges of each view-graph along with observed noisy relative orientations in each epoch. During testing all the edges were kept active. The parameters that yielded the minimum validation loss were kept for evaluation. All the baselines including the proposed networks were evaluated on an Intel Core i7 CPU.

5. Results

Experiments were carried out on synthetic as well as real datasets to demonstrate the true potential of our approach.

Baseline methods We evaluated NeuRoRA against the following baseline methods (also described in Section 2):

- Chatterjee and Govindu [5]: The latest implementation with the default parameters and cost function in the shared scripts³ were employed. We also utilized their

²<https://pytorch-geometric.readthedocs.io>

³<http://www.ee.iisc.ac.in/labs/cvl/research/rotaveraging/>

Table 2. Results of Rotation averaging on a test synthetic dataset. The average angular error on all the view-graphs in our dataset is displayed. The proposed method NeuRoRA is remarkably faster than the baselines while producing better results. NeuRoRA-*v2* is a variation of NeuRoRA where the initialization from CleanNet is fine-tuned in a two-step of FineNet. There is no GPU implementations of [5] and [16] available, thus these methods are excluded from the runtime comparisons on cuda.

	Angular Error			Runtime (seconds)		
	mn	md	rms	cpu	cuda	
Baseline Methods						
Chatterjee [5]	2.17°	1.25°	4.55	5.38s	(1×)	—
Weiszfeld [16]	3.35°	1.02°	9.74	50.92s	(0.11×)	—
Proposed Methods						
CleanNet-SPT + [5]	2.11°	1.26°	4.04	5.41s	(0.99×)	—
CleanNet-SPT + [16]	1.74°	1.01°	3.53	50.36s	(0.11×)	—
NeuRoRA	1.45°	0.74°	3.53	0.21s	(24×)	0.0016s
NeuRoRA- <i>v2</i>	1.30°	0.68°	3.28	0.30s	(18×)	0.0021s
Other Methods						
CleanNet-SPT	2.93°	1.47°	5.34	0.11s	(47×)	0.0007s
SPT-FineNet	3.00°	1.57°	6.12	0.11s	(47×)	0.0007s
SPT-FineNet + [5]	2.12°	1.26°	4.11	5.41s	(0.99×)	—
SPT-FineNet + [16]	1.78°	1.01°	3.95	50.36s	(0.11×)	—
NeuRoRA + [5]	2.11°	1.26°	4.04	5.51s	(0.97×)	—
NeuRoRA + [16]	1.73°	1.01°	3.51	50.46s	(0.10×)	—

mn: mean of the angular error, md: median of the angular error, rms: root mean square angular error, and cpu: the runtime of the method on a cpu. MethodA + MethodB: MethodB is initialized by the solution of MethodA

evaluation strategy to compare the predicted orientations with the ground-truth orientations.

- Weiszfeld algorithm [16]: The algorithm is straightforward but computationally expensive and we only ran it for 50 iterations of Weiszfeld algorithm of ℓ_1 averaging.

Although DISCO [9] is similar to the proposed method in a sense that it detects outliers to get a good initialization and then fine-tunes the initialization (by a non-linear optimization), however, it is computationally very expensive. It takes approximately an hour for a view-graph with 463 cameras and 11.4K pairwise observations. Further, DISCO produces inferior results to [5] and [16]⁴. Therefore it was excluded from the baseline methods for evaluation. We also ran the graph cleaning network (CleanNet) followed by bootstrapping initial orientation (using SPT) as a baseline CleanNet-SPT, and ran SPT on the noisy graph followed by fine-tuning network (FineNet) as another baseline SPT-FineNet. Note that the proposed network NeuRoRA takes CleanNet-SPT as an initialization and then fine-tunes the initialization in a single step by FineNet. NeuRoRA-*v2* is a variation of the proposed method where the initialization from CleanNet-SPT is fine-tuned in two steps of FineNet, *i.e.* the output of FineNet in the first step is fed as an initialization of FineNet in the second step. Although the proposed method is easy to reproduce, we released⁵ the code to facilitate research in the direction of learning-based

⁴A detailed comparison can be found in [5]

⁵<https://github.com/pulak09/NeuRoRA>

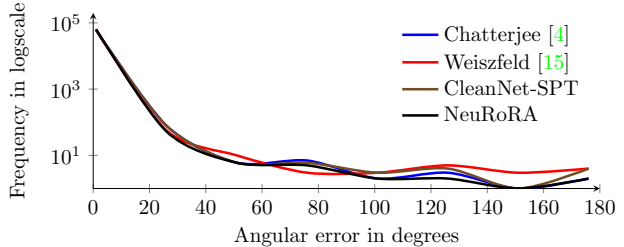


Figure 4. Histograms of the angular errors (log scale) in degrees of the predicted orientations by different methods in synthetic dataset. Notice that the optimization methods have thicker tails than the proposed method. This indicates a superior performance of our method over the conventional optimization methods.

solutions for geometric problems.

Synthetic dataset We carefully designed a synthetic dataset that closely resembles the real-world datasets. Since the amount of noise in observed relative measurements changes with the sensor type (*e.g.* camera device), the structure of the connections in the view-graphs and the outlier ratios are varied with the scene (Figure 2). We sampled (1) the number of cameras, (2) the sparsity in the view-graph, (3) the distributions of pairwise relative orientation noise, and (4) the percentage of outlier edges in each view-graph separately. A single view-graph was generated as follows: (1) the number of cameras were sampled in the range 250 – 1000 and their orientations were generated randomly on a horizontal plane (yaw only), (2) pairwise edges and corresponding relative orientations were randomly introduced between the cameras that amounted to (10 – 30)% of all possible pairs, (3) the relative orientations were then corrupted by a noise with a std σ where σ is chosen uniformly in the range (5° – 30°) once for the entire view-graph, and the directions are chosen randomly on the vertical plane (to emulate realistic distributions 2), and (4) the relative orientations were further corrupted by (0 – 30)% of outliers with random orientations. Further, no sophisticated rule was employed to determine the connections among cameras, for example, cameras with similar absolute orientations are potentially connected. The good performance of our network depicts that the choice is not critical, and a random connection is employed instead. Our synthetic dataset consisted of 1200 sparse view-graphs. The dataset was divided into training (80%), validation (10%), and testing (10%).

The results are furnished in Table 2 and in Figure 4. The average angular error on all the view-graphs in the dataset is displayed. The proposed method NeuRoRA performs remarkably well compared to the baselines in terms of accuracy and speed. NeuRoRA-*v2* further improves the results. Overall, Chatterjee [5] performs well but the performance does not improve with a better initialization. Weiszfeld [16] improves the performance

Table 3. Results of MRA on real datasets. The proposed method NeuRoRA is much faster than the baselines while producing overall similar or better results. The number of cameras, for which ground-truths are available, is shown within brackets.

Datasets			Chatterjee [5]				Weiszfeld [16]				CleanNet-SPT + Weiszfeld [16]				NeuRoRA			
Name	#cameras	#edges	mn	md	rms	cpu	mn	md	rms	cpu	mn	md	rms	cpu	mn	md	rms	cpu
Alamo	627(577)	97206	4.16	1.06	12.68	20.47s	4.89	1.38	15.95	84.03s	4.46	1.19	13.65	84.01s	4.94	1.16	16.09	2.19s
Ellis Island	247(227)	20297	2.87	0.51	10.36	2.49s	4.36	1.04	16.50	8.97s	3.47	1.05	13.27	9.02s	2.59	0.64	12.82	0.35s
Gendermen Market	742(677)	48144	37.56	7.71	67.30	11.08s	29.37	9.56	49.53	53.71s	12.98	6.79	27.60	53.71s	4.51	2.94	9.60	0.53s
Madrid Metropolis	394(341)	23784	6.97	1.29	17.28	3.28s	7.51	2.67	17.01	14.53s	7.40	2.69	16.47	14.45s	2.55	1.13	6.59	0.25s
Montreal NotreDam	474(450)	52424	1.54	0.51	7.45	9.17s	2.17	0.78	9.32	41.58s	1.87	0.77	8.66	41.39s	1.23	0.64	2.67	1.03s
NYC Library	376(332)	20680	3.04	1.35	6.99	4.86s	3.87	2.18	8.65	14.40s	3.50	2.27	6.52	14.06s	1.90	1.18	2.89	0.27s
Notre Dame	553(553)	103932	3.53	0.65	14.61	23.33s	4.79	0.88	19.17	80.86s	4.27	0.69	16.25	79.43s	1.65	0.68	6.37	2.05s
Piazza Del Popolo	354(338)	24710	4.06	0.89	8.41	3.30s	4.87	1.38	11.73	16.78s	4.63	1.41	9.27	16.72s	3.05	0.79	9.01	0.42s
Piccadilly	2508(2152)	319257	6.97	2.95	19.30	449.09s	26.44	7.52	46.68	1328.12s	10.09	4.30	22.71	1328.72s	4.75	1.91	13.96	5.96s
Roman Forum	1134(1084)	70187	3.15	1.59	10.21	20.21s	4.85	1.87	17.22	115.07s	3.66	2.58	8.44	115.68s	2.39	1.31	5.52	1.37s
Tower of London	508(472)	23863	3.94	2.43	9.06	1.95s	4.74	2.99	10.58	17.16s	4.25	2.98	8.50	17.18s	2.63	1.46	5.78	0.37s
Trafalgar	5433(5058)	680012	3.59	2.02	9.83	858.40s	15.68	11.37	24.95	5572.22s	9.63	4.47	23.96	5169.97s	5.33	2.25	15.71	15.55s
Union Square	930(789)	25561	9.33	3.93	22.44	6.80s	40.97	10.31	61.46	42.80s	7.98	5.16	16.77	42.66s	5.98	2.01	17.61	0.68s
Vienna Cathedral	918(836)	103550	8.29	1.28	27.84	48.14s	11.72	1.99	36.68	158.39s	4.41	1.85	12.56	158.55s	3.91	1.54	9.93	2.12s
Yorkminster	458(437)	27729	3.51	1.60	8.41	4.03s	5.73	2.03	17.30	32.04s	3.56	2.02	7.45	32.03s	2.52	0.99	6.55	0.45s
Acropolis	463(463)	11421	1.14	0.70	1.71	1.59s	0.66	0.37	1.10	15.04s	0.58	0.33	0.88	15.04s	0.89	0.55	1.31	0.21s
Arts Quad	5530(4978)	222044	4.82	3.57	8.92	116.18s	34.44	23.18	49.76	1886.42s	27.30	7.02	54.64	1891.23s	27.51	7.32	54.83	5.01s
San Francisco	7866(7866)	101512	3.68	3.41	4.27	15.27s	18.84	16.41	21.89	1349.56s	18.31	13.47	23.31	1355.47s	17.63	12.62	22.57	2.67s
TNotre Dame	715(715)	64678	1.07	0.42	3.55	10.69s	1.40	0.66	4.53	72.50s	2.78	1.59	6.22	72.50s	1.71	0.70	5.93	1.42s

mn: mean of the angular error (in deg), md: median of the angular error (in deg), rms: root mean square angular error, and cpu: the runtime of the method on a cpu (in sec).

with a better initialization given by CleanNet-SPT, but, it can not improve the solution further given an even better initialization by NeuRoRA. This validates our initial claim about learning the patterns in the data by a neural network and the proposed NeuRoRA has thus demonstrated a potential solution to this specific application. Notice that the proposed NeuRoRA is three orders of magnitude faster with a GPU than the baseline methods.

Real dataset We summarize the real datasets and display in Table 3. There are a total of 19 publicly available view-graphs with observed noisy relative orientations and the ground-truth absolute orientations. The ground-truth orientations were obtained by applying incremental bundle adjustment [2] on the view-graphs. The *TNotre Dame* dataset is shared by Chatterjee *et al.* [5]⁶. The *Artsquad* and *San Francisco* datasets are provided by DISCO [9]⁷. The rest of the view-graphs are publicly shared by 1DSFM [29]⁸. In Table 3, #edges represents the number of edges, and #camera represents the number of cameras in the view-graph. The ground-truth orientations are available for some of those cameras (indicated in parenthesis) and the training, validation and testing are performed only on those cameras.

Due to limited availability of real datasets for training, we employed network parameters pre-trained on the above synthetic dataset and further fine-tuned on the real datasets in round-robin fashion. We evaluated (*i.e.* validated and tested) each real view-graph in Table 3 one at a time while the rest of the view-graphs were used to fine-tune the network. Overall, the proposed NeuRoRA outperformed the baseline optimization methods for this task in terms of ac-

curacy and efficiency. The *Artsquad* and *San Francisco* datasets have larger view-graphs than the rest of the real datasets, moreover, they potentially have different orientation patterns (as shared from a different source [9], also see Figure 2). Thus, the performance of NeuRoRA falls short to Chatterjee *et al.* [5] only on those sequences, but still produces better results than Weiszfeld [16]. The *Acropolis* dataset is quite clean on which the Weiszfeld [16] algorithm performs exceptionally well. In the rest of the datasets, NeuRoRA produces better or similar results. Nonetheless, the proposed NeuRoRA is much faster than the baselines.

6. Discussion

We have proposed a graph-based neural network for absolute orientation regression of a number of cameras from their observed relative orientations. The proposed network is exceptionally faster than the strong optimization-based baselines while producing better results on most datasets. The outstanding performance of the current work and the relevant neural networks for test-time optimization leads to the following question: “*can we then replace all the optimizations in robotics / computer vision by a suitable neural network-based regression?*” The answer is obviously *No*. For instance, if an optimization at test-time requires solving a simpler convex cost with a few parameters to optimize, a naive gradient descent will find the globally optimal parameters, while a network-based regression would only estimate sub-optimal parameters. To date, neural nets have been proven to be consistently better at solving pattern recognition problems than solving a constraint optimization problems. A few neural network-based solutions are proposed recently that can exploit the patterns in the data while solving a test-time optimization. Therefore the current work

⁶<http://www.ee.iisc.ac.in/labs/cvl/research/rotaveraging/>

⁷<http://vision.soic.indiana.edu/projects/disco/>

⁸<http://www.cs.cornell.edu/projects/1dsfm/>

also opens up many questions related to the right tool for a specific application.

References

- [1] Jonas Adler and Ozan Öktem. Solving ill-posed inverse problems using iterative deep neural networks. *Inverse Problems*, 33(12):124007, 2017. [2](#)
- [2] Sameer Agarwal, Noah Snavely, Steven M Seitz, and Richard Szeliski. Bundle adjustment in the large. In *Proceedings of ECCV*, pages 29–42. Springer, 2010. [8](#)
- [3] Yasuhiro Aoki, Hunter Goforth, Rangaprasad Arun Srivatsan, and Simon Lucey. Pointnetlk: Robust & efficient point cloud registration using pointnet. In *Proceedings of CVPR*, pages 7163–7172, 2019. [2](#)
- [4] Ramaswamy Chandrasekaran and Arie Tamir. Open questions concerning weiszfeld’s algorithm for the fermat-weber location problem. *Mathematical Programming*, 44(1-3):293–295, 1989. [2](#)
- [5] Avishek Chatterjee and Venu Madhav Govindu. Robust relative rotation averaging. *TPAMI*, 40(4):958–972, 2017. [1](#), [2](#), [3](#), [4](#), [6](#), [7](#), [8](#)
- [6] Avishek Chatterjee and Venu Madhav Govindu. Efficient and robust large-scale rotation averaging. In *Proceedings of ICCV*, pages 521–528. IEEE, 2013. [2](#)
- [7] Yutian Chen, Matthew W Hoffman, Sergio Gómez Colmenarejo, Misha Denil, Timothy P Lillicrap, Matt Botvinick, and Nando de Freitas. Learning to learn without gradient descent by gradient descent. In *Proceedings of ICML*, pages 748–756. JMLR. org, 2017. [2](#)
- [8] Ronald Clark, Michael Bloesch, Jan Czarnowski, Stefan Leutenegger, and Andrew J Davison. Learning to solve non-linear least squares for monocular stereo. In *Proceedings of ECCV*, pages 284–299, 2018. [2](#)
- [9] David Crandall, Andrew Owens, Noah Snavely, and Dan Huttenlocher. Discrete-continuous optimization for large-scale structure from motion. In *Proceedings of CVPR*, pages 3001–3008. IEEE, 2011. [2](#), [3](#), [7](#), [8](#)
- [10] Anders Eriksson, Carl Olsson, Fredrik Kahl, and Tat-Jun Chin. Rotation averaging and strong duality. In *Proceedings of CVPR*, pages 127–135, 2018. [1](#), [2](#)
- [11] Johan Fredriksson and Carl Olsson. Simultaneous multiple rotation averaging using lagrangian duality. In *Proceedings of ACCV*, pages 245–258. Springer, 2012. [1](#)
- [12] Ravi Garg, Vijay Kumar BG, Gustavo Carneiro, and Ian Reid. Unsupervised cnn for single view depth estimation: Geometry to the rescue. In *Proceedings of ECCV*, pages 740–756. Springer, 2016. [1](#)
- [13] Justin Gilmer, Samuel S Schoenholz, Patrick F Riley, Oriol Vinyals, and George E Dahl. Neural message passing for quantum chemistry. In *Proceedings of ICML*, pages 1263–1272. JMLR. org, 2017. [5](#)
- [14] Venu Madhav Govindu. Combining two-view constraints for motion estimation. In *Proceedings of CVPR*, volume 2, pages II–II. IEEE, 2001. [2](#)
- [15] Venu Madhav Govindu. Lie-algebraic averaging for globally consistent motion estimation. In *Proceedings of CVPR*, volume 1, pages I–I. IEEE, 2004. [2](#)
- [16] Richard Hartley, Khurram Aftab, and Jochen Trunpf. L1 rotation averaging using the weiszfeld algorithm. In *Proceedings of CVPR*, pages 3041–3048. IEEE, 2011. [2](#), [4](#), [6](#), [7](#), [8](#)
- [17] Richard Hartley, Jochen Trunpf, Yuchao Dai, and Hongdong Li. Rotation averaging. *IJCV*, 103(3):267–305, 2013. [1](#), [2](#), [3](#), [4](#)
- [18] Refael Hassin and Arie Tamir. On the minimum diameter spanning tree problem. *Information processing letters*, 53(2):109–111, 1995. [6](#)
- [19] Alex Kendall, Matthew Grimes, and Roberto Cipolla. Posenet: A convolutional network for real-time 6-dof camera relocalization. In *Proceedings of ICCV*, pages 2938–2946. IEEE, 2015. [1](#)
- [20] Elias Khalil, Hanjun Dai, Yuyu Zhang, Bistra Dilikina, and Le Song. Learning combinatorial optimization algorithms over graphs. In *Proceedings of NIPS*, pages 6348–6358, 2017. [2](#)
- [21] Rainer Kümmeler, Giorgio Grisetti, Hauke Strasdat, Kurt Konolige, and Wolfram Burgard. g 2 o: A general framework for graph optimization. In *Proceedings of ICRA*, pages 3607–3613. IEEE, 2011. [1](#)
- [22] Yuying Li. A newton acceleration of the weiszfeld algorithm for minimizing the sum of euclidean distances. *Computational Optimization and Applications*, 10(3):219–242, 1998.
- [23] Zhaoyang Lv, Frank Dellaert, James M Rehg, and Andreas Geiger. Taking a deeper look at the inverse compositional algorithm. In *Proceedings of CVPR*, pages 4581–4590, 2019. [2](#)
- [24] Etienne Mouragnon, Maxime Lhuillier, Michel Dhome, Fabien Dekeyser, and Patrick Sayd. Generic and real-time structure from motion using local bundle adjustment. *Image and Vision Computing*, 27(8):1178–1193, 2009. [1](#)
- [25] Charles R Qi, Hao Su, Kaichun Mo, and Leonidas J Guibas. Pointnet: Deep learning on point sets for 3d classification and segmentation. In *Proceedings of CVPR*, pages 652–660, 2017. [1](#), [2](#)
- [26] Chengzhou Tang and Ping Tan. Ba-net: Dense bundle adjustment network. *ICLR 2019*, 2019. [2](#)
- [27] Robert Endre Tarjan. Sensitivity analysis of minimum spanning trees and shortest path trees. *Information Processing Letters*, 14(1):30–33, 1982. [6](#)
- [28] Kyle Wilson, David Bindel, and Noah Snavely. When is rotations averaging hard? In *Proceedings of ECCV*, pages 255–270. Springer, 2016. [1](#), [2](#)
- [29] Kyle Wilson and Noah Snavely. Robust global translations with ldsfm. In *Proceedings of ECCV*, pages 61–75. Springer, 2014. [1](#), [3](#), [8](#)

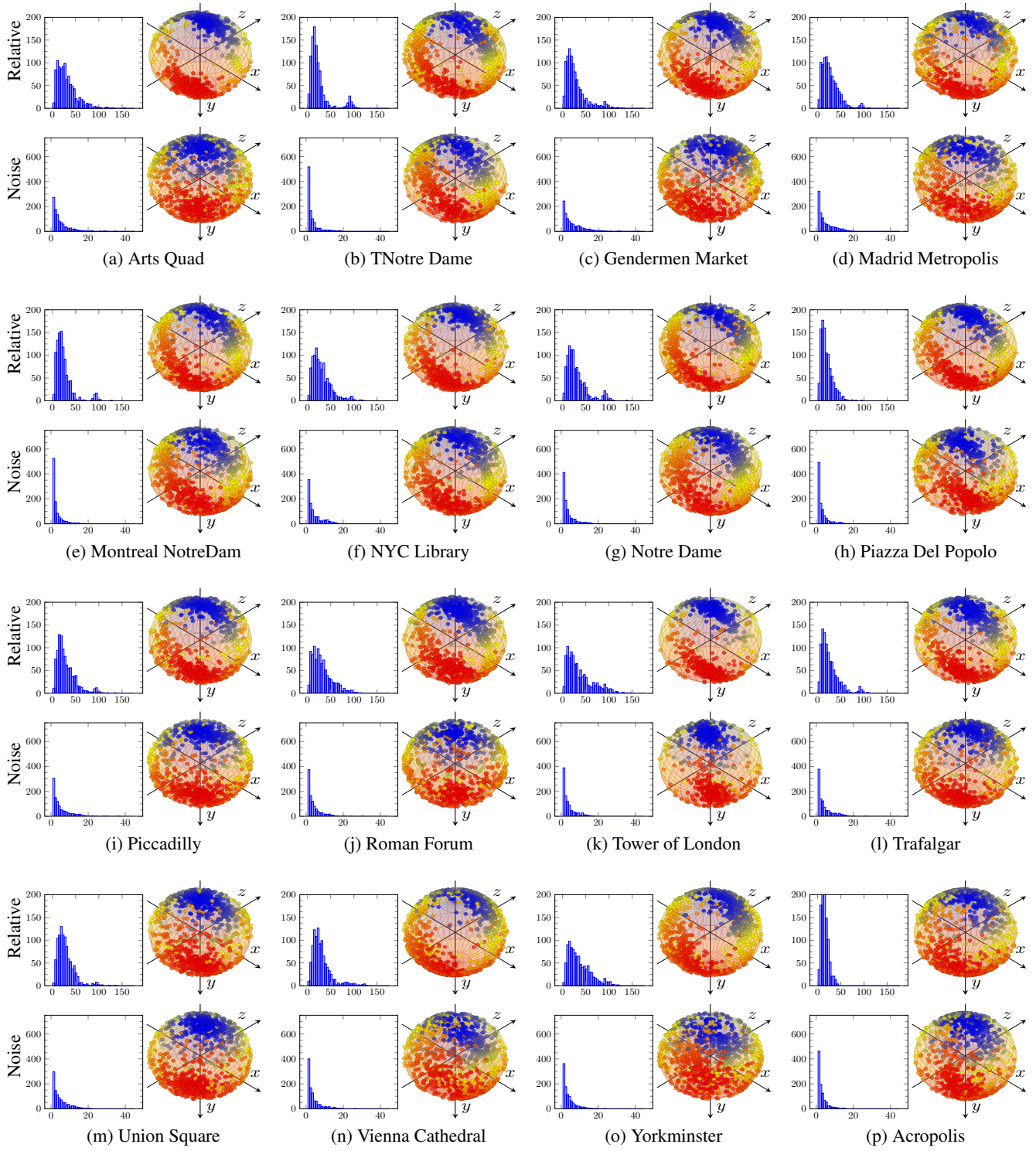


Figure 5. More examples of Figure 2(a)-(c) are displayed. The angle and axes of sampled observed relative orientations (first row) and the same of noise (second row) in real datasets (for clarity only 1000 random samples) are displayed. The noise orientation is calculated from the ground-truth absolute orientations and the observed relative orientations. We plotted histograms of the magnitudes of the angles in degrees and the axes of the orientations. Notice that the axes of the sampled relative and noise orientations are distributed mostly along a vertical ring rather than uniformly on a unit ball.